RSC Advances

ROYAL SOCIETY OF CHEMISTRY

www.rsc.org/advances

TOC

MOF-derived microporous carbon (ZIF-C) exhibits considerably higher capacity and better reversibility than mesoporous CMK-3 as anode material of Na-ion batteries.

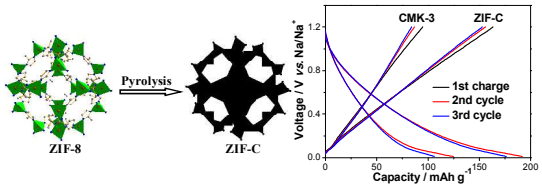

MOF-derived microporous carbon as a better choice for Na-ion batteries than mesoporous CMK-3

Qunting Qu,[a,b] Jiaojiao Yun,[b] Zhongming Wan,[b] Huiyuan Zheng,[b] Tian Gao,[b] Ming Shen,[c] Jie Shao,*[a] and Honghe Zheng*[b]*

[a] *College of Chemistry, Chemical Engineering and Material Science, Soochow University, Suzhou Jiangsu 215006, China*
[b] *College of Physics, Optoelectronics and Energy & Collaborative Innovation Center of Suzhou Nano Science and Technology, Soochow University, Suzhou Jiangsu 215006, China.*
[c] *Huasheng Chemical Corporation, Zhangjiagang, Jiangsu 215635, China*
E-mail: qtqu@suda.edu.cn; shaojie@suda.edu.cn; hhzheng@suda.edu.cn

Keywords: carbon, micropores, metal organic frameworks, pyrolysis, Na-ion batteries

Abstract: A metal-organic framework, 2-methylimidazole zinc salt (ZIF-8), is prepared through a scalable solution-precipitation method. Microporous carbon (ZIF-C) with a homogeneous pore size of 0.5 nm is obtained through direct pyrolysis of ZIF-8. Mesoporous carbon (CMK-3) with an average pore size of about 4.0 nm is achieved using SBA-15 as hard template. Microporous ZIF-C exhibits considerably higher capacity and better reversibility than mesoporous CMK-3 as anode material of Na-ion batteries. In addition, it is found that the microporous ZIF-C can greatly reduce the irreversible capacity loss (reductive decomposition of electrolyte) of the first cycle and enhance the reversibility of Na^+ storage during the subsequent cycles.

Introduction

Li-ion batteries have achieved great success in the fields of portable electronic devices, whereas their large-scale application in electric grids is still being hindered by their high-cost and limited resources. Because of the natural abundance, cheapness, and electrochemical activity of Na^+-related materials, Na-ion batteries are considered as the most promising alternatives to Li-ion batteries.[1-7] By analogy with Li-ion batteries, various electrode materials that are capable of storing Li^+ have been investigated to store Na^+.[8-10] Graphite is the dominant anode material of Li-ion batteries. However, graphite can only accommodate a very small amount of Na^+ resulting from the large size of Na^+.[11-14] Disordered carbon with low graphitic degree was recently reported to possess a more decent capacity for Na^+ storage.[12-17] Hollow carbon nanowires prepared through pyrolyzation of hollow polyaniline nanowires exhibit a reversible capacity of 251 mAh g^{-1}.[13] Polystyrene-templated hollow carbon microspheres possess excellent cycling stability and rate capability as anode materials of Na-ion batteries.[12] Mesoporous carbon obtained by the nanocasting method using silica as template manifests significantly improved performance and kinetics for Na^+ storage as compared with graphite.[14] Nonetheless, the influence of porous structure on the Na^+ storage capability of carbon materials has not been clearly understood. Accurate control of the porous structure of carbon materials and comparative researches on their Na^+ storage performance would not only favor a better understanding of Na^+ storage mechanism but also help exploration of superior carbon anode materials.

Direct pyrolysis of metal organic frameworks (MOFs)[18] was recently found to be an

easy and effective method to synthesize microporous carbon with a narrow pore-size distribution and extremely high surface area. These microporous carbon already exhibited appealing performance in energy storage systems like Li-ion batteries, fuel cells, Li-sulfur batteries, and supercapacitors.[19-26] To the best of our knowledge, the potential application of MOFs-derived microporous carbon in Na-ion batteries has not been exploited. In addition, whether the micropores are beneficial for the reversible Na^+ storage/release of carbon or not is a question remaining unanswered. In this work, microporous carbon polyhedrons (ZIF-C) with a homogeneous pore size of 0.5 nm is synthesized through pyrolysis of an easily available zeolitic imidazolate framework, 2-methylimidazole zinc salt (ZIF-8). Another mesoporous carbon (CMK-3) with an average pore size of about 4 nm is achieved using SBA-15 as hard template and glucose as carbon source. Comparative results on their Na^+ storage performance indicate that microporous ZIF-C can greatly weaken the reductive decomposition of electrolyte in the first cycle and result in a higher reversible capacity than mesoporous CMK-3.

Experimental Section

Synthesis of ZIF-8 polyhedrons and SBA-15

The synthesis procedures of ZIF-8 are as follows. First, 175 mg of $Zn(CH_3COO)_2$ and 263 mg of 2-methylimidazole were dissolved separately in methanol to generate two clear solutions. The two solutions were then mixed together, stirred for 5 min, and aged at room temperature for 24 hours. At last, the white precipitates were collected,

washed carefully with ethanol, and dried at 60^{o}C.

For the synthesis of SBA-15, 2 g of Pluronic P123 ($EO_{20}PO_{70}EO_{20}$) was dissolved in 60 mL of 2 M HCl solution at 38 ^{o}C. 4.2 g of tetraethylorthosilicate was then added to the above solution under vigorous stirring. The mixture was stirred for 24 h at 38 ^{o}C, and then hydrothermally treated at 100 ^{o}C for another 24 h in an autoclave. The precipitates were filtered, dried, and finally calcined at 550 ^{o}C in air.

Synthesis of microporous ZIF-C and mesoporous CMK-3

Microporous ZIF-C carbon was obtained through pyrolysis of ZIF-8 polyhedrons operated at a temperature of 930 ^{o}C under N_2 atmosphere. The obtained black samples were washed at last using 2 M HCl solution to remove residual inorganic components. For the synthesis of mesoporous CMK-3, 0.5 g of SBA-15 was dispersed in 2.5 mL of aqueous solution containing 0.625 g of sucrose and 0.07 g of H_2SO_4. The mixture was then heated at 100 ^{o}C for 6 h, followed by another 6 h at 160 ^{o}C. The sucrose infiltration was then repeated with a 2.5 mL aqueous solution containing 0.4 g of sucrose and 0.045 g of H_2SO_4. Finally, the composite was carbonized at 930 ^{o}C under N_2 atmosphere, and the silica template was removed using 2 M NaOH solution.

Materials characterization

Scanning electron microscope (SEM) images were obtained using Philip XL30 scanning electron microscope operated at 25 kV. Transmission electron microscope (TEM) images were obtained using FEI Tecnai G-20 microscope. X-ray diffraction (XRD) patterns were collected using a Rigaku D/MAX-IIA X-ray diffractometer with Cu *K*α radiation. Field-emission Raman spectra were measured through JobinYvon

LabRAM HR800 Raman spectrometer with an excitation wavelength of 514 nm. The N_2 adsorption/desorption isotherms were obtained using Micromeritics ASAP2020 V4.0 apparatus with liquid nitrogen at 77 K.

Electrochemical testing

The working electrode slurry was prepared by dispersing the mixture of active material (ZIF-C or CMK-3), carbon black, and poly(vinylidene fluoride) (PVDF) binder with a weight ratio of 8/1/1 in N-methylpyrrolidone. The slurry was spread onto copper foil and dried at 60 ^{o}C for 2 h in an oven. The obtained copper foil was then punched into small disks with diameter of 13 mm. The mass loading of active material on each disk is about 1.5 mg cm^{-2}. The electrode disks were dried at 120 ^{o}C overnight before use. CR2032-type coin cells were assembled using Na disk as the counter electrode and 1 M $NaClO_4$ dissolved in propylene carbonate (PC) solvent as electrolyte.

Results and discussion

ZIF-8, whose molecular structure is shown in Fig. 1a, is a metal organic framework utilizing the coordination reaction between Zn^{2+} ions and nitrogen atoms on five-membered imidazole rings. During the pyrolysis of ZIF-8 at 930^{o}C under N_2 atmosphere, the organic ligands of ZIF-8 were supposed to crosslink together and then being carbonized, while Zn^{2+} ions were reduced to metallic Zn that would vaporize at temperature above 907^{o}C (boiling point of Zn). The procedures for the preparation of CMK-3 (Fig. 1b) include the synthesis of SBA-15 template, infiltration

of organic precursors into pores of template, and removal of template, which are complex and time-consuming. Therefore, the MOFs-derived method for the preparation of carbon materials is much simpler than the template-based method.

The morphologies of the obtained materials were investigated through SEM. As shown in Fig. 2a, the ZIF-8 precursors are composed of uniform polyhedrons, which is the morphology commonly observed for ZIF-8.[27] The average size of these polyhedrons is about 300 nm, much smaller than that of micrometer-scaled polyhedrons reported due to the different preparation conditions.[26] After pyrolysis, both the shape and dimension of polyhedrons are perfectly maintained (Fig. 2b and S1). So the final product is called ZIF-C carbon polyhedrons. SEM image of CMK-3 (Fig. 2c) exhibits the typical rod-like structure, indicating that the sucrose precursors were successfully impregnated into the mesopores of SBA-15 template during preparation. In addition, it is obviously observed that the surface of ZIF-C polyhedrons is smoother than that of CMK-3. High-resolution TEM image taken at the edge of one typical ZIF-C polyhedron (Fig. 2d) shows that it possesses numerous graphene nanosheets and interconnected nanopores all over the particle surface.

XRD patterns of ZIF-C and CMK-3 are shown in Fig. 2e. The two broad peaks at around 25^{o} and 44^{o} are characteristic of the (002) and (101) crystalline planes of graphite. According to Scherrer equation, the dimension of nanocrystallites should be inversely proportional to the full width at half maximum (FWHM) of the diffraction peaks. In the case of the (002) peak representing the layer-by-layer structure of graphite, the FWHM of ZIF-C is slightly wider than that of CMK-3, meaning that the

crystallites size of ZIF-C in the direction of c-axis should be smaller as compared with CMK-3. In other words, the graphitic degree of ZIF-C is lower than that of CMK-3. Raman spectra of ZIF-C and CMK-3 are shown in Fig. 2f. The relative ratios of D bands to G bands are important parameters for understanding the crystallization degree of graphitic carbon. The I_D/I_G ratios of ZIF-C and CMK-3 are 1.2 and 1.0, respectively, further suggesting that the graphitic degree of ZIF-C is lower than that of CMK-3.

The porous structure of ZIF-C and CMK-3 was analyzed through N_2 adsorption/desorption isotherms. As shown in Fig. 3a, ZIF-C presents the Type I isotherms with a sharp uptake at low pressure and a smooth plateau at middle-to-high pressure, which are characteristic of microporous material.[28] The pore size distribution curve of ZIF-C (inset in Fig. 3a) was obtained by analyzing the adsorption branch of isotherms using Horvath-Kawazoe method.[29] ZIF-C exhibits an extremely narrow pore size distribution centered at 0.5 nm, further validating that ZIF-C consists of homogenous micropores. In contrast, Type IV isotherms are observed for CMK-3 (Fig. 3b). The distinct hysteresis loop at high pressure signifies the presence of mesopores. Barrett-Joyner-Halenda (BJH) method was adopted to analyze the pore size distribution of mesoporous material. The pore size distribution curve of CMK-3 (inset in Fig. 3b) presents one sharp peak at approximately 4.0 nm, which also suggests the mesoporous structure of CMK-3. The specific surface areas of ZIF-C and CMK-3 were determined to be 1251 and 1056 $m^2\ g^{-1}$, respectively, suggesting the highly developed porosity of the two materials. The well-defined pore size of

microporous ZIF-C and mesoporous CMK-3 enables us to evaluate the effect of different porous structure on the Na^+ storage performance of carbon materials.

The initial discharge curves of ZIF-C and CMK-3 electrodes (vs. Na/Na^+) at a current density of 50 mA g^{-1} and their corresponding differential capacity curves are shown in Fig. 4a and 4b, respectively. By comparison, the differences between the two discharge curves mainly lie in the following three aspects. First, ZIF-C exhibits a particular short plateau at about 1.3 V, which is also embodied by the small peak in differential capacity curve. It is believed that the reaction of Na^+ with the functional groups of ZIF-C should contribute to this part of capacity. In contrast, no obvious discharge plateau is observed at this voltage for CMK-3. The reason can be ascribed to the nitrogen-rich precursor of ZIF-8, which endows ZIF-C with unique nitrogen-containing functional groups (Fig. S1). The elemental analysis results show that the nitrogen content of ZIF-C is about 3.1 wt%, while CMK-3 contains no nitrogen due to the absence of nitrogen source during preparation. Second, the discharge plateau of ZIF-C at about 0.6 V is considerably shorter compared to that of CMK-3, which is also reflected by the smaller peak of ZIF-C in differential capacity curves. This part of capacity is related to the reductive decomposition of PC-based electrolyte or the formation of solid electrolyte interphase (SEI) film.[16] The shorter plateau of ZIF-C in this potential range indicates that the decomposition of electrolyte on ZIF-C electrode should be less severe than that occurs on CMK-3 electrode. However, it occurs to us that the slightly higher surface area and lower graphitic degree of ZIF-C than CMK-3 as well as the presence of nitrogen-containing groups in

ZIF-C are supposed to result in a more severe reaction of electrolyte. A high surface area of the electrode material usually can increase the contact areas between the electrode and electrolyte, leading to a more drastic reaction of electrolyte on the electrode surface. A case in point is the high-surface-area graphene, which presents a considerable larger irreversible capacity than graphite in the first cycle due to the serious decomposition of electrolyte.[30] The lower graphitic degree of ZIF-C as indicated by the XRD patterns and Raman spectra means that ZIF-C possesses more disordered or defective carbon atoms resulting from its large quantity of micropores. These defective carbon atoms mostly located at the edges of graphene nanoplates could work as the active sites for the reduction decomposition of electrolyte. Nitrogen-doped carbon materials have already been proven to possess improved electrochemical or catalytic activity as compared to the undoped ones.[31] The nitrogen-containing groups in ZIF-C could also contribute to the reduction reaction of electrolytes. Therefore, the reasons for the less severe decomposition of electrolyte on ZIF-C should be related to the different pore-size distribution and morphology of ZIF-C and CMK-3. A schematic is shown in Fig. 4c to illustrate the contact of micropores or mesopores with electrolytes. Penetration of solvent molecules (PC) into the mesopores (4 nm) is easy, leading to a drastic electrolyte reaction at the inner surface of CMK-3. The extremely small pore-size of microporous ZIF-C (0.5 nm) can accommodate only a very small amount of solvent molecules, which reduces the electrode/electrolyte contact area and gives rise to a weaker reduction reaction of electrolyte. In addition, as compared with the smooth surface of ZIF-C polyhedrons,

the rough surface of CMK-3 nanorods may provide more active sites and deteriorate the reduction reaction of electrolyte. Third, the initial discharge capacity of ZIF-C (851 mAh g^{-1}) is obviously smaller than that of CMK-3 (1204 mAh g^{-1}), indicating that the reduction reaction of electrolyte accounts for the major part of capacity in the first discharge.

The typical charge/discharge curves of ZIF-C and CMK-3 electrodes during the following cycles in the voltage range of 1.2-0.01 V are shown in Fig. 4d. Both ZIF-C and CMK-3 exhibit sloping voltage (vs. capacity) profiles, similar to those porous carbon materials for application in Na-ion batteries.[12, 14] Remarkably, the long plateaus at about 0.6 V shown in Fig. 4a disappear during the second and third discharge, suggesting that the reductive decomposition of electrolyte is effectively prevented due to the formation of SEI film in the first discharge, which can greatly decrease the irreversible capacity loss of the following cycles. The Na^+ storage capacity of ZIF-C and CMK-3 during the following cycles should be based on the insertion or adsorption of Na^+ into/on carbon layers and interaction of Na^+ with impurity atoms.[14] The initial charge capacities of ZIF-C and CMK-3 are 164 and 95 mAh g^{-1}, respectively. Such a significant discrepancy between the reversible capacities of ZIF-C and CMK-3 can be related to their different discharge behaviors in the first cycle. It has been found that, the reversible capacity of graphite-base anode for Li^+ storage declined during the long-term cycles because the SEI film became thicker.[32-33] In the present case, the severe decomposition of electrolyte on CMK-3 electrode during the first discharge would result in the formation of a thick SEI film

covering on its surface, which could preclude the reversible adsorption or intercalation of Na^+ and decrease its Na^+ storage capacity during the following cycles. As a result, CMK-3 exhibits a much lower reversible capacity than ZIF-C. In addition, it should be pointed out that the reversible capacity of ZIF-C is comparable to or slightly higher than those of poly(styrene)- or silica-templated porous carbon materials.[12, 14]

The reversible capacities of ZIF-C and CMK-3 at various current densities are shown in Fig. 4e. When the current density increases to 500 mA g^{-1}, 129 and 56 mAh g^{-1} of capacity are retained for ZIF-C and CMK-3, respectively, suggesting the excellent rate behaviors of these carbon materials for Na^+ storage. The reasons should be associated with the highly porous structure of ZIF-C and CMK-3, which renders a fast electrochemical reaction mainly occurring on the carbon surface. The capacity variations of ZIF-C and CMK-3 during extended cycles at a current density of 50 mA g^{-1} are shown in Fig. 4f. ZIF-C manifests good cycling stability with 136 mAh g^{-1} of capacity retained in the 50th cycle. After about 10 cycles, the coulombic efficiencies of ZIF-C and CMK-3 (inset in Fig. 4f) stabilize at about 96% and 94%, respectively, suggesting that the reversibility of Na^+ uptake/release on ZIF-C electrode is slightly better than that on CMK-3 electrode. Although the optimization of electrolyte systems may further improve the cycling performance of these carbon anodes,[34-35] the results shown in this study clearly demonstrate the superiority of MOF-derived microporous ZIF-C over mesoporous CMK-3 for Na^+ storage.

Conclusion

Microporous carbon polyhedrons with an extremely narrow pore-size distribution are synthesized through direct pyrolysis of ZIF-8. In contrast to the silica-templated mesoporous carbon, the microporous carbon manifests much higher reversible capacity and coulombic efficiency during repeated charge/discharge for Na^+ storage. It is believed that the extremely small pore size of ZIF-C can significantly weaken the reductive decomposition of electrolyte. The template-free synthesis and superior performance of ZIF-C make it a promising anode material for Na-ion batteries.

Acknowledgements

This work was supported by National Natural Science Foundation of China (NSFC No. 21203133, 21301124, 21473120, and 51272168) and The Natural Science Foundation of Jiangsu Province (BK2012186).

1 H. Pan, Y.-S. Hu and L. Chen, *Energy Environ. Sci.*, 2013, **6**, 2338-2360.
2 V. Palomares, P. Serras, I. Villaluenga, K. B. Hueso, J. Carretero-Gonzalez and T. Rojo, *Energy Environ. Sci.*, 2012, **5**, 5884-5901.
3 M. D. Slater, D. Kim, E. Lee and C. S. Johnson, *Adv. Funct. Mater.*, 2013, **23**, 947-958.
4 S.-W. Kim, D.-H. Seo, X. Ma, G. Ceder and K. Kang, *Adv. Energy Mater.*, 2012, **2**, 710-721.
5 D. Su, X. Xie and G. Wang, *Chem. Eur. J.*, 2014, **20**, 3192-3197.
6 Y.-X. Wang, S.-L. Chou, D. Wexler, H.-K. Liu and S.-X. Dou, *Chem. Eur. J.*, 2014, **20**, 9607-9612.
7 J. Shao, Y. Ding, X. Li, Z. Wan, C. Wu, J. Yang, Q. Qu and H. Zheng, *J. Mater. Chem. A*, 2013, **1**, 12404-12408.
8 B. Qu, C. Ma, G. Ji, C. Xu, J. Xu, Y. S. Meng, T. Wang and J. Y. Lee, *Adv. Mater.*, 2014, **26**, 3854-3859.
9 L. David, R. Bhandavat and G. Singh, *ACS Nano*, 2014, **8**, 1759-1770.
10 H. Zhu, Z. Jia, Y. Chen, N. Weadock, J. Wan, O. Vaaland, X. Han, T. Li and L. Hu, *Nano Lett.*, 2013, **13**, 3093-3100.
11 S. Y. Hong, Y. Kim, Y. Park, A. Choi, N.-S. Choi and K. T. Lee, *Energy Environ. Sci.*, 2013, **6**, 2067-2081.
12 K. Tang, L. Fu, R. J. White, L. Yu, M.-M. Titirici, M. Antonietti and J. Maier, *Adv.*

Energy Mater., 2012, **2**, 873-877.
13 Y. Cao, L. Xiao, M. L. Sushko, W. Wang, B. Schwenzer, J. Xiao, Z. Nie, L. V. Saraf, Z. Yang and J. Liu, *Nano Lett.*, 2012, **12**, 3783-3787.
14 S. Wenzel, T. Hara, J. Janek and P. Adelhelm, *Energy Environ. Sci.*, 2011, **4**, 3342-3345.
15 K.-l. Hong, L. Qie, R. Zeng, Z.-q. Yi, W. Zhang, D. Wang, W. Yin, C. Wu, Q.-j. Fan, W.-x. Zhang and Y.-h. Huang, *J. Mater. Chem. A*, 2014, **2**, 12733-12738.
16 S. Komaba, W. Murata, T. Ishikawa, N. Yabuuchi, T. Ozeki, T. Nakayama, A. Ogata, K. Gotoh and K. Fujiwara, *Adv. Funct. Mater.*, 2011, **21**, 3859-3867.
17 L. Fu, K. Tang, K. Song, P. A. van Aken, Y. Yu and J. Maier, *Nanoscale*, 2014, **6**, 1384-1389.
18 M. Hu, J. Reboul, S. Furukawa, N. L. Torad, Q. Ji, P. Srinivasu, K. Ariga, S. Kitagawa and Y. Yamauchi, *J. Am. Chem. Soc.*, 2012, **134**, 2864-2867.
19 B. Liu, H. Shioyama, T. Akita and Q. Xu, *J. Am. Chem. Soc.*, 2008, **130**, 5390-5391.
20 A. Morozan and F. Jaouen, *Energy Environ. Sci.*, 2012, **5**, 9269-9290.
21 K. Xi, S. Cao, X. Peng, C. Ducati, R. Vasant Kumar and A. K. Cheetham, *Chem. Commun.*, 2013, **49**, 2192-2194.
22 G. Xu, B. Ding, L. Shen, P. Nie, J. Han and X. Zhang, *J. Mater. Chem. A*, 2013, **1**, 4490-4496.
23 S.-L. Li and Q. Xu, *Energy Environ. Sci.*, 2013, **6**, 1656-1683.
24 W. Chaikittisilp, K. Ariga and Y. Yamauchi, *J. Mater. Chem. A*, 2013, **1**, 14-19.
25 W. Chaikittisilp, M. Hu, H. Wang, H.-S. Huang, T. Fujita, K. C. W. Wu, L.-C. Chen, Y. Yamauchi and K. Ariga, *Chem. Commun.*, 2012, **48**, 7259-7261.
26 H. B. Wu, S. Wei, L. Zhang, R. Xu, H. H. Hng and X. W. Lou, *Chem. Eur. J.*, 2013, **19**, 10804-10808.
27 N. L. Torad, M. Hu, Y. Kamachi, K. Takai, M. Imura, M. Naito and Y. Yamauchi, *Chem. Commun.*, 2013, **49**, 2521-2523.
28 S. Xin, L. Gu, N.-H. Zhao, Y.-X. Yin, L.-J. Zhou, Y.-G. Guo and L.-J. Wan, *J. Am. Chem. Soc.*, 2012, **134**, 18510-18513.
29 B. Zhang, X. Qin, G. R. Li and X. P. Gao, *Energy Environ. Sci.*, 2010, **3**, 1531-1537.
30 A. Abouimrane, O. C. Compton, K. Amine and S. T. Nguyen, *J. Phys. Chem. C*, 2010, **114**, 12800-12804.
31 X. Ma, G. Ning, C. Qi, C. Xu and J. Gao, *ACS Appl. Mater. Interfaces*, 2014, **6**, 14415-14422.
32 V. A. Agubra and J. W. Fergus, *J. Power Sources*, 2014, **268**, 153-162.
33 L. Tan, L. Zhang, Q. Sun, M. Shen, Q. Qu and H. Zheng, *Electrochim. Acta*, 2013, **111**, 802-808.
34 A. Ponrouch, E. Marchante, M. Courty, J.-M. Tarascon and M. R. Palacin, *Energy Environ. Sci.*, 2012, **5**, 8572-8583.
35 S. Komaba, T. Ishikawa, N. Yabuuchi, W. Murata, A. Ito and Y. Ohsawa, *ACS Appl. Mater. Interfaces*, 2011, **3**, 4165-4168.

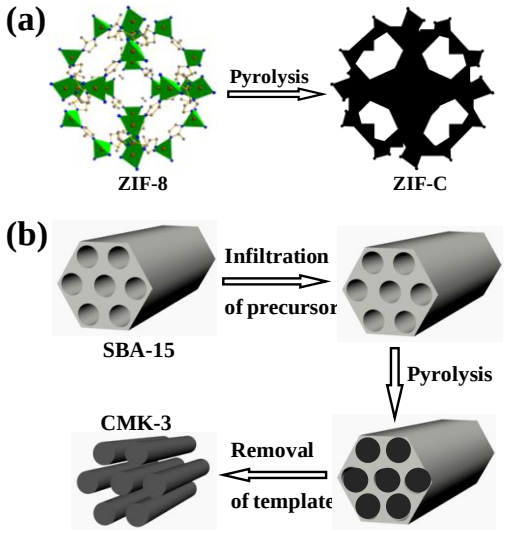

Fig. 1 Schematic illustrations of the formation of (a) ZIF-C and (b) CMK-3.

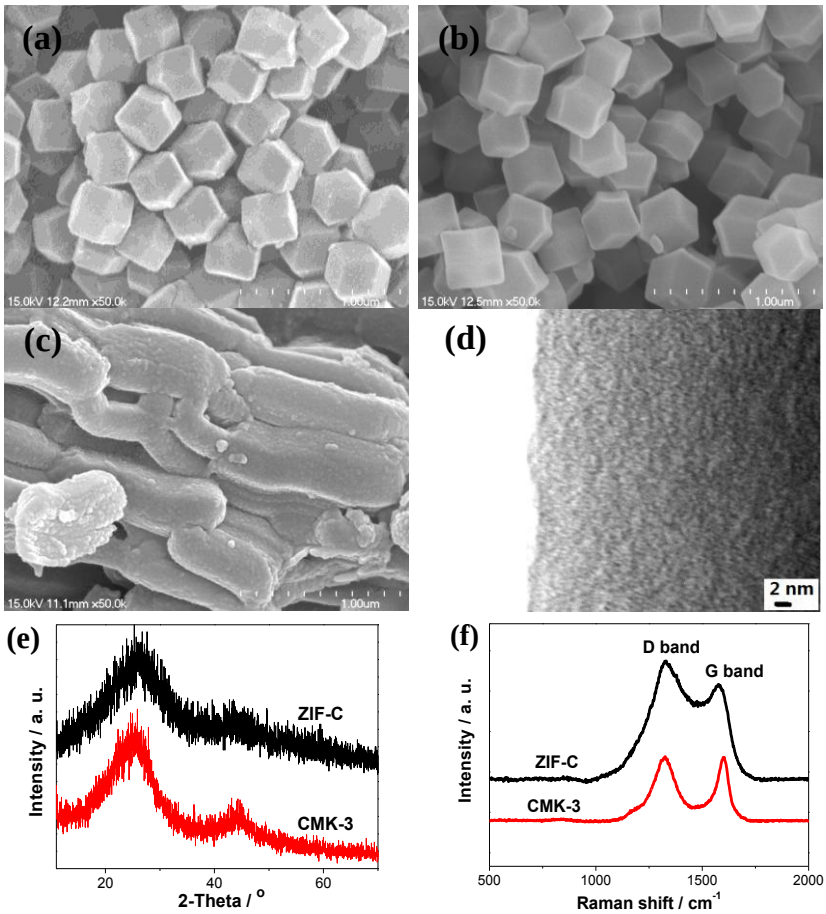

Fig. 2 SEM images of (a) ZIF-8 precursor and (b) ZIF-C carbon polyhedrons obtained through pyrolysis of ZIF-8. (c) SEM image of CMK-3 obtained using SBA-15 as hard template. (d) High-resolution TEM image of ZIF-C taken at the edge of one typical polyhedron. (e) XRD patterns of ZIF-C and CMK-3. (f) Raman spectra of ZIF-C and CMK-3.

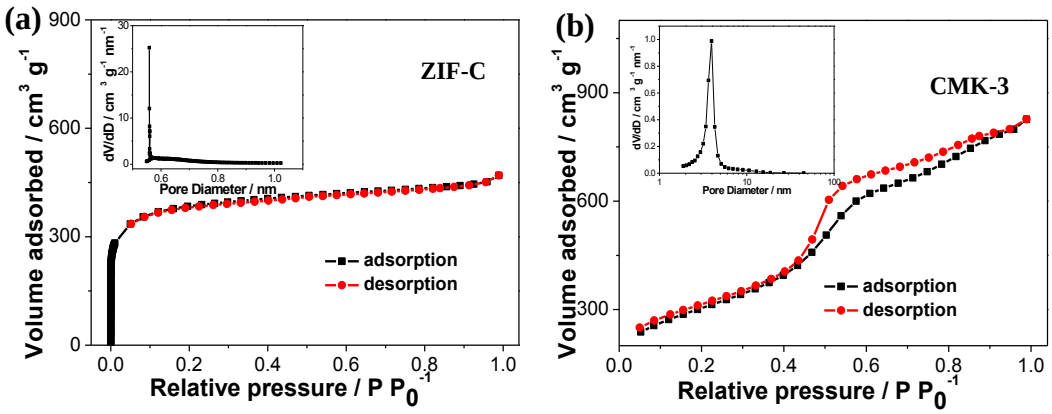

Fig. 3 N_2 adsorption/desorption isotherms of (a) ZIF-C and (b) CMK-3. The corresponding pore-size distribution curves are shown in the insets.

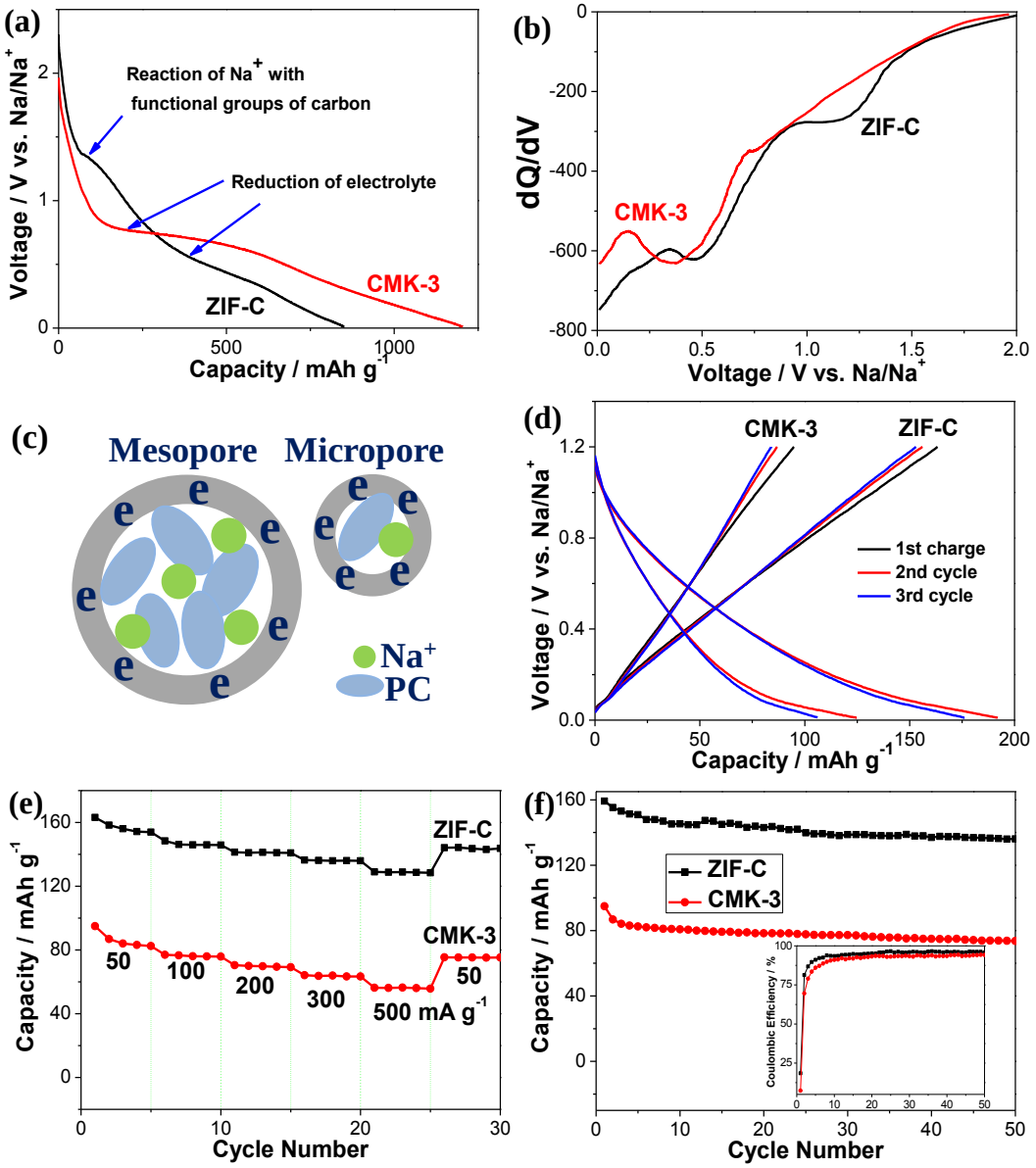

Fig. 4 (a) The initial discharge curves and (b) the corresponding differential capacity curves of ZIF-C and CMK-3 electrodes. (c) Schematics illustrating the contact conditions of mesopores or micropores with electrolytes. (d) The typical discharge/charge curves of ZIF-C and CMK-3 electrodes during the following several cycles. (e) Rate behaviors of ZIF-C and CMK-3 electrodes. (f) Capacity variations of ZIF-C and CMK-3 electrodes during long-term cycles. The coulombic efficiency during repeated discharge/charge is shown in the inset.